

Numerical Investigation of Combustion and Soot Formation Processes in Turbulent Nonpremixed Flame

Hoo-Joong Kim and Yong-Mo Kim

Department of Mechanical Engineering, Hanyang University

Seoul, KOREA

ymkim@mail.hanyang.ac.kr

Abstract

In order to incorporate the soot formation and oxidation processes, we employed the two-variable approach and the related source terms represent the soot nucleation, coagulation, surface growth and oxidation. For the simulation of the axi-symmetric turbulent reacting flows, the pressure-velocity coupling is handled by the pressure based finite volume method. The laminar flamelet model is adopted to account for the turbulence-chemistry interaction as well as to calculate the thermo-chemical properties and the proper soot source terms. The numerical and physical models used in this study successfully predict the essential features of the combustion processes and soot formation characteristics.

Introduction

In practical combustion devices such as industrial furnaces, gas turbines, or internal combustion engine, most of them use the hydrocarbon fuels and deviate from the ideal conditions under which the combustion of fuel leads to carbon dioxide and water. Therefore, soot is generated as a by-product in the region where the local concentration of oxygen is not sufficient to convert the fuel into water and carbon dioxide. Since this soot emission causes the severe environmental damages and human health problems, there is need for better understanding of the processes that are responsible for the formation and oxidation of soot.

While intensive research have been performed over the last decade in understanding and modeling soot formation, there is no universal theory nor models that are applicable to different fuels and a wide range of flow conditions. These are mainly caused by its complexity such as PAH chemical kinetics and surface reaction. Brooke and Moss[9] investigated axisymmetric turbulent methane/air jet flames at atmosphere and elevated pressure. There are quite detailed measured data sets in terms of mean mixture fraction, mean temperature, and soot volume fraction. So we selected this experiment as the benchmark case.

In the present study, we used the laminar flamelet approach to model the turbulent combustion processes. Laminar flamelet model views the turbulent flame as an ensemble of stationary laminar diffusion flamelets which are stretched and distorted by the turbulent flow. This approach gives us the advantage that is the detailed information of intermediate species and radicals. For the investigated methane/air flame, a library of flamelets has been calculated. The chemical model consists of 32 chemical species and 177 chemical reaction for the methane/air flame. The rate coefficients were taken from GRI-Mech 2.11 and we did not include the NOx production mechanism of original chemical mechanism. The stationary solutions were stored in a library containing profiles of temperature, density, and mass fractions of all species in dependence on mixture fraction and scalar dissipation rate. We also employed the two variable soot modeling proposed by Lindstedt et. al[7] because of its simplicity and treated acetylene as a soot precursor. The numerical and physical models used in this study successfully predict the essential features of the combustion processes and soot formation characteristics in the reacting flow field.

Flow field modeling

The density-weighted Navier-Stokes equation, k-ε turbulent model equation, energy equation, and mean and variance of mixture fraction equations are employed to predict the turbulent reacting flows in cylindrical coordinate and represented as following form.

$$\frac{\partial}{\partial t}(\bar{\rho}\phi) + \frac{\partial}{\partial x_j}(\bar{\rho}\tilde{u}\phi) = \frac{\partial}{\partial x_j}\left(\Gamma_\phi \frac{\partial\phi}{\partial x_j}\right) + S_\phi \quad (1)$$

where ϕ includes mean axial and radial velocity, mean enthalpy, turbulent kinetic energy and dissipation rate, mean and variance of mixture fraction and Γ_ϕ and S_ϕ represent the diffusion coefficient and source term of its equation, respectively. In this study, we used the same diffusion coefficients and source terms in Ref [1].

The energy conservation equation is solved in terms of enthalpy and its source terms include the effect of thermal radiation. In the present study, we assume that the flame is optically thin so that radiation source term can be determined locally only by emission. With this assumption of the optically thin limit, the radiative heat loss rate per unit volume can be expressed as

$$Q_{rad} = 4\sigma \left(P_k \cdot a_{p,k}\right) (T^4 - T_b^4) \quad (2)$$

where σ is the Stefan-Boltzmann constant, P_k is the partial pressure of species k, T is the local flame temperature and T_b is the background temperature. The Planck mean absorption coefficient, $a_{p,k}$ for radiating gas species k are taken from the curve fit value in computational submodel section of International Workshop on Measurement

and Computation of Turbulent Nonpremixed Flames[2].

The governing equations are solved using a control-volume based finite difference method on an unsteady fashion. The present formulation is based on a curvilinear general coordinate with a non-staggered grid. Second order accurate central differencing scheme is used for the diffusion terms. To reduce numerical diffusion, second order TVD upwind scheme[3] for convection terms is implemented. The pressure-velocity coupling is handled by the improved PISO algorithm.[4]

Laminar flamelet approach

The laminar flamelet model views the turbulent flame as an ensemble of stationary laminar diffusion flamelets which are stretched and distorted by the turbulent flow. In laminar flamelets, all thermodynamic scalar quantities are unique function in the mixture fraction and scalar dissipation rate. One can obtain the species and energy equation transformed into flamelet coordinate, namely mixture fraction(Z) and scalar dissipation rate(χ) space, by introducing a Crocco coordinate transformation. Using these transformed equations, we can construct the flamelet library. In the present study, we used the transformed equations which have variable Lewis number and scalar dissipation rate in mixture fraction space.[5]

For the investigated methane/air flame, a library of flamelets has been calculated. To achieve greater precision in the calculations, a flamelet code with an adaptive grid was used. The chemical model consist of 32 chemical species and 177 chemical reaction for the methane/air flame. The rate coefficients were taken from GRI-Mech 2.11 and we did not include the NOx production mechanism of original chemical mechanism. The stationary solutions were stored in a library containing profiles of temperature, density, and mass fractions of all species in dependence on mixture fraction and scalar dissipation rate.

With the calculated laminar flamelet library, the mean thermo- chemical properties in turbulent reacting flow can be calculated by following manner, if the probability density function(PDF) is known.

$$\tilde{\phi} = \int_0^1 \int_0^1 \phi(Z, \chi) P(Z, \chi) dZ d\chi \quad (3)$$

where $P(Z, \chi)$ is the joint PDF of mixture fraction and scalar dissipation rate. If the mixture fraction, Z and scalar dissipation rate, χ are statistically independent each other, the joint probability function can be simply written as

$$P(Z, \chi) = P(Z) \cdot P(\chi) \quad (4)$$

To avoid complications, we used the presumed PDF approach which imply making assumption of the shape of the PDF. The most commonly used PDF for the mixture fraction is the beta function distribution and for the scalar dissipation rate, the log-normal distribution[6].

$$P(Z) = \frac{Z^{a-1} (1-Z)^{b-1}}{\int_0^1 Z^{a-1} (1-Z)^{b-1} dZ} \quad \text{where } a = \tilde{Z} \left(\frac{\tilde{Z}(1-\tilde{Z})}{\tilde{Z}^2} - 1 \right) \quad b = (1-\tilde{Z}) \left(\frac{\tilde{Z}(1-\tilde{Z})}{\tilde{Z}^2} - 1 \right) \quad (5)$$

where mean and variance of mixture fraction are provided by the solution of its transport equations.

$$P(\chi) = \frac{1}{\chi \sigma \sqrt{2\pi}} \exp \left[-\frac{1}{2\sigma^2} (\ln \chi - \mu)^2 \right] \quad \text{where } \tilde{\chi} = \exp(\mu + 0.5\sigma^2) \quad \sigma^2 = 2.0 \quad (6)$$

where the mean scalar dissipation rate is modeled as follow :

$$\tilde{\chi} = C_\chi \frac{\tilde{\epsilon}}{k} \tilde{Z}^2 \quad C_\chi = 2.0 \quad (7)$$

Modeling of soot formation and oxidation

Selecting the laminar flamelet model as the turbulent combustion model, we have an advantage that is the ability to give us the information of the intermediate species and radicals. In the flamelet soot modeling, instead of the soot volume fraction, the rate of soot volume fraction is expressed as a function of the mixture fraction and the scalar dissipation rate. In the present study, we used the two-equation model proposed by Lindstedt et. al[7] because of its simplicity. In this approach, the Favre averaged transport equation of soot particle number density and soot mass fraction are written as the form of equation (1) if we insert the proper scalar variables and its source terms. For soot number density equation ($\phi_n = n/\rho$) and soot mass fraction ($\phi_v = \rho_{\text{soot}} f_v / \rho = Y_{C(s)}$), the source terms are :

$$\begin{aligned} S_{\phi_v} &= r_i M_{C(s)} + r_{ii} \rho M_{C(s)}^{1/3} Y_{C(s)}^{1/3} n^{1/3} - r_{iii} \rho M_{C(s)}^{1/3} Y_{C(s)}^{1/3} n^{1/3} \\ S_{\phi_n} &= r_{iv} - r_v \rho^2 M_{C(s)}^{-1/6} Y_{C(s)}^{1/6} n^{11/6} \end{aligned} \quad (8)$$

here, the first, second and third source term of soot mass fraction equation represent nucleation, surface growth and O₂ oxidation, respectively. The first and second source term of soot number density equation is the nucleation and coagulation rate. The following Arrhenius type expressions have been proposed by Lindstedt et. al[7] for each reaction rate.

$$r_i = 1.35 \times 10^6 \exp(-20634/T) [C_2 H_2] \quad r_{ii} = 5.00 \times 10^2 \exp(-12079/T) f(p) [C_2 H_2]$$

$$r_{iii} = 1.78 \times 10^{-2} T^{1/2} \exp(-19628/T) f'(p) [O_2]$$

$$r_{iv} = \frac{2}{C_{\min}} N_A r_i \quad r_v = 2C_a \left(\frac{6M_{C(s)}}{\pi \rho_{C(s)}} \right)^{1/6} \left(\frac{6kT}{\pi \rho_{C(s)}} \right)^{1/2} \quad (9)$$

$$f(p) = \pi \left(\frac{6M_{C(s)}}{\pi \rho_{C(s)}} \right)^{2/3} \quad f'(p) = \frac{f(p)}{M_{C(s)}}$$

where T is gas temperature, $M_{C(s)}$ is molar mass of soot (12.011 kg/kmol), $\rho_{C(s)}$ is soot density (1800 kg/m³), C_{\min} is the number of carbon atoms in the incipient carbon particle (9×10^4), C_a is a coagulation rate constant (3), N_A is Avogadro's number (6.022×10^{26} particles/kmol) and k is Boltzmann constant (1.381×10^{-23} J/K).

We also implemented the OH soot oxidation rate proposed by Bradley et. al [8]. This reaction rate is added in source term of soot mass fraction equation and given as follow :

$$r_{OH} = -0.36 T^{1/2} f'(p) [OH] \rho M_{C(s)}^{1/3} Y_{C(s)}^{2/3} n^{1/3} \quad (10)$$

Results and discussion

We have chosen the experimental measurements of Moss et. al [9] to validate the present model. The experimental conditions are that temperature is 290K for both the fuel and air streams and pressure is 1atm. Fuel is injected through a nozzle of 4.07mm at a speed of 20.3m/s. The air stream has a mass flow rate of 707g/min to the chamber. The combustion chamber diameter is 155mm. The calculation of the governing equation is performed in the cylindrical coordinate system. The governing equations in this computational domain were discretized by grid system which has 98 and 100 points in axial and radial direction, respectively.

At first, we investigated the scalar field, especially temperature field, in order to validate the models used in the present study. Figure 1 represents the radial profiles of mean temperature at some axial locations (i.e. $z=150, 200, 250, 300, 350, 425$ mm). The calculation of thermo-chemical scalar quantities is carried out using the flamelet library and presumed PDF. In the region of $z > 350$ mm, the over predicted temperature exists near the centerline. However, the predicted values of temperature agree with the measured value and calculated profiles also have good prediction capability of the radial location of peak temperature at each axial location. So, we concluded that the laminar flamelet model has good prediction ability for calculating the scalar fields such as temperature etc.

Figure 2 shows the fields of temperature and acetylene which has been treated as soot precursor. Temperature has its maximum value in the flame tip region and peak temperature exist along the stoichiometric line. Acetylene has its maximum concentration in the upstream region ($z \approx 280$ mm) of maximum temperature region. The overall distribution of acetylene shows that higher acetylene concentration is in the fuel rich region.

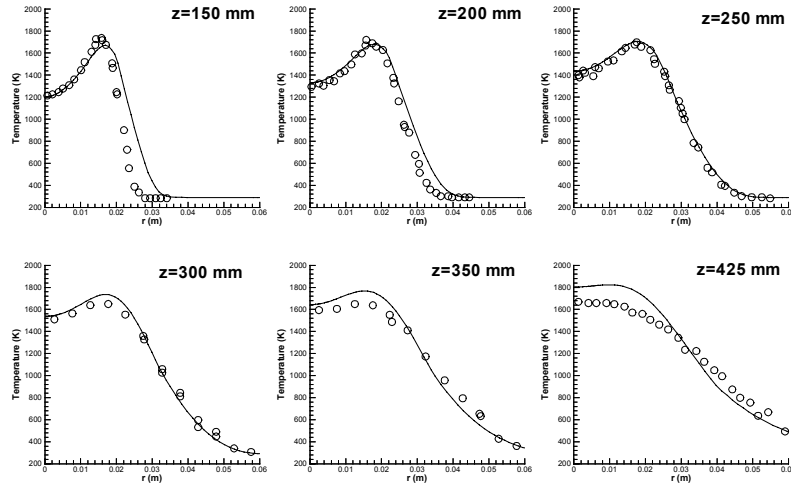


Fig.1 Radial profiles of mean temperature at some axial positions. (Symbols : measurements, Lines : predictions)

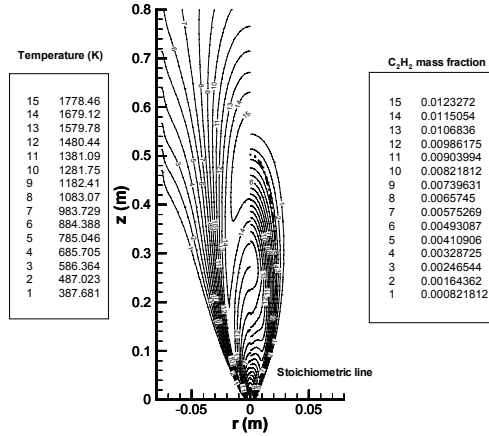


Fig.2 Temperature and acetylene mass fraction fields. Dashdot line denotes the stoichiometric line.

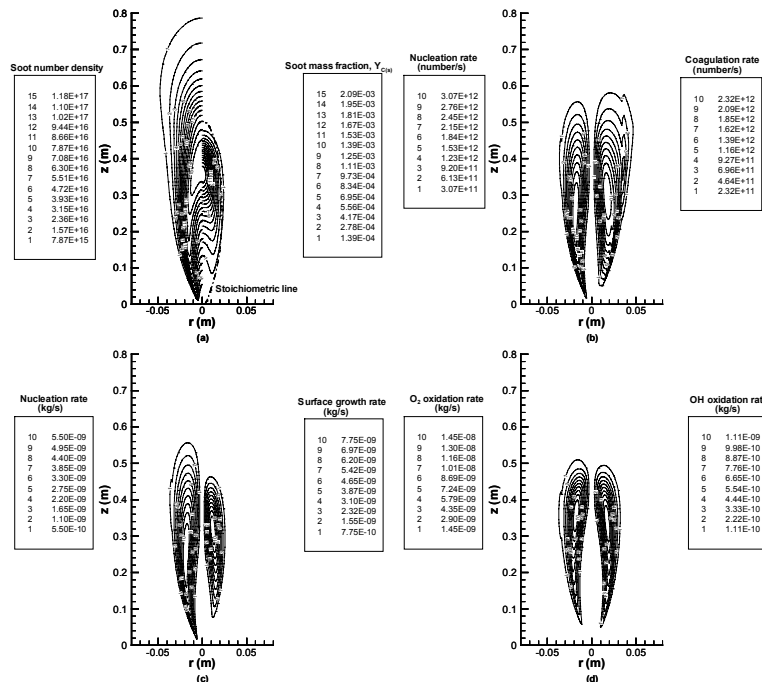


Fig.3 The distribution of soot number density, soot mass fraction and its source terms. (a) Soot number density and soot mass fraction. Dashdot line denotes the stoichiometric line. (b) Nucleation and coagulation rate of soot number density. (c) Nucleation and surface growth rate of soot mass fraction. (d) O₂ and OH oxidation rate of soot mass fraction.

The soot number density, mass fraction and its source terms are shown in Figure 3. Since soot nucleation rate is not only dependent on acetylene concentration but also temperature, it has its maximum value not in the region of maximum acetylene concentration but in the region ($z \approx 260\text{mm}$, $r \approx 15\text{mm}$) where high temperature and acetylene concentration coexist. Soot surface growth rate has maximum value in the slightly downstream of maximum nucleation rate region. Because it is not only dependent on the acetylene concentration but also proportional to the soot surface area, high number density leads to the high surface growth rate. O₂ and OH oxidation rate is also proportional to the soot surface area so that they have maximum rates in the high soot number density region. OH oxidation rate has peak values along the high temperature region due to its high concentration in that region. Soot particle is oxidized by O₂ at more radial location than OH oxidation location. The generated soot particles are transported to the downstream region and its size is increased by soot surface growth and decreased by surface oxidation. Near $z = 370\text{mm}$, soot mass fraction has maximum value. As soot particle move toward downstream and radial region of its maximum mass fraction place, soot particle is oxidized and soot mass fraction is decreased rapidly. Most of soot particles exist in the fuel rich condition. Since coagulation rate is not only proportional to temperature and number density but also proportional to the square root of soot diameter, it has maximum value in slightly downstream of maximum nucleation rate location. We understand that maximum coagulation location does not coincide with maximum soot number region and this mainly results from the decrease of soot diameter by surface oxidation.

Figure 4 shows the radial profiles of soot volume fraction at $z=350$ and 425 mm. Only considering soot nucleation and surface growth, we have large over-prediction in entire radial range. The predicted value is approaching to the measured value due to including soot surface oxidation. The soot oxidation rate is higher in downstream than upstream region. Because OH soot oxidation rate is much less than O_2 oxidation rate, the effect of OH soot oxidation on the soot volume fraction is small. But OH oxidation results in the decrease of soot volume fraction near the centerline. The prediction of soot volume fraction has good level for comparison with the measured value. But overprediction is in the upstream and underprediction is in the downstream. The width of soot distribution is underpredicted because the oxidation rate is higher than the surface growth rate. Treating acetylene as a soot precursor mainly causes these results. So, the predictive capability could be improved if we account for chemical species including benzene and PAH as a soot precursor and use the improved soot surface reaction model such as HACA(Hydrogen Abstraction C_2H_2 Addition) mechanism and PAH condensation.

Conclusions

The numerical modeling of turbulent combustion and soot formation is presented. This study utilized the density weighted Navier-Stokes equations and standard k- ϵ turbulent model equations to model the turbulent flow field and mixture fraction equation, laminar flamelet model and presumed PDF(beta function for mixture fraction and log-normal function for scalar dissipation rate) approach to solve the mean reaction rate. We also employed the two-variable model representing soot number density and soot mass fraction and its source terms which include the acetylene concentration as soot precursor.

The models used in the present study give us good agreement with the experimental distributions and have good capability to predict scalar quantity such as temperature. Nucleation rate has maximum value in the region where high temperature and acetylene concentration coexist due to its dependency on temperature and acetylene concentration. The generated soot particles transport to the downstream and are oxidized by oxygen and OH species. As soot particles go through the oxidation zone, the soot mass fraction and particle diameter are decreased rapidly. Maximum coagulation location does not coincide with maximum soot number region and this mainly results from the decrease of soot diameter by surface oxidation. Most of soot is in the fuel rich condition. The predicted profiles of soot volume fraction have the relatively good conformity with experimental data. But they are noticeably overpredicted in the upstream and underpredicted in the downstream. The width of soot distribution is underestimated because the oxidation rate is higher than the surface growth rate.

References

1. Kim, S.K. and Kim, Y.M., "Prediction of Detailed Structure and NO_x Formation Characteristics in Turbulent Nonpremixed Hydrogen Jet", *Combust. Sci. and Tech.*, Vol.156, pp.107-137 (2000).
2. <http://www.ca.sandia.gov/tdf/Workshop/Submodels.html>
3. Chakravarthy, S.R., and Osher, S., AIAA-85-0363, 23rd Aerospace Sciences Meeting, Reno, NV (1985).
4. Kim, Y.M., Chen, C.P., Ziebarth, J.P., and Chen, Y.S., *Numerical Heat Transfer*, vol.25, pp.21-42 (1994)
5. Pitsch, H. and Peters, N., "A Consistent Flamelet Formulation for Non-Premixed Combustion Considering Differential Diffusion Effects", *Combust. and Flame*, Vol. 114, pp26-40 (1998)
6. Lentini, D., "Assessment of the Stretched Laminar Flamelet Approach for Nonpremixed Turbulent Combustion", *Combust. Sci. and Tech.*, Vol. 100, pp.95-122 (1994).
7. Fairweather, M., Jones, W.P., and Lindstedt, R.P., "Predictions of Radiative Transfer from a Turbulent Reacting Jet in a Cross-Wind", *Combust. and Flame*, Vol. 89, pp.45-63 (1992)
8. Bradley, D., Dixon-Lewis, G., El-Din Habik and Mushi, E.M.J., 20th Symposium (International) on Combustion, The Combustion Institute, p.931 (1984).
9. Brookes, S. and Moss, J. B., "Measurement of Soot Production and Thermal Radiation from Confined Turbulent Jet Diffusion Flames of Methane", *Combust. and Flame*, Vol. 116, pp.49-61 (1999)

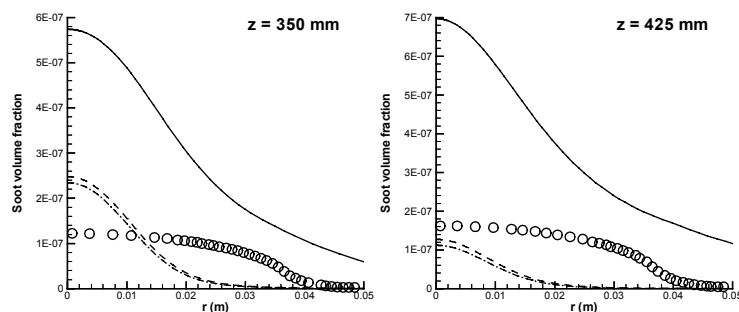


Fig. 4 Radial profiles of soot volume fraction at some axial locations. Symbol denotes the measured value. Lines denote the prediction; solid (including nucleation and surface growth), dashed (including nucleation, surface growth and O_2 oxidation), dashdot (including nucleation, surface growth, O_2 oxidation and OH oxidation)